Research article

Fatih Balli, Mansoor A. Sultan, Aytekin Ozdemir and Jeffrey Todd Hastings*

An ultrabroadband 3D achromatic metalens

https://doi.org/10.1515/nanoph-2020-0550
Received September 30, 2020; accepted January 5, 2021;
published online January 25, 2021

Abstract: We design and fabricate ultra-broadband achromatic metalenses operating from the visible into the shortwave infrared, 450–1700 nm, with diffraction-limited performance. A hybrid 3D architecture, which combines nanoholes with a phase plate, allows realization in low refractive index materials. As a result, two-photon lithography can be used for prototyping while molding can be used for mass production. Experimentally, a 0.27 numerical aperture (NA) metalens exhibits 60% average focusing efficiency and 6% maximum focal length error over the entire bandwidth. In addition, a 200 μm diameter, 0.04 NA metalens was used to demonstrate achromatic imaging over the same broad spectral range. These results show that 3D metalens architectures yield excellent performance even using low-refractive index materials, and that two-photon lithography can produce metalenses operating at visible wavelengths.

Keywords: achromat; metalens; nanohole; two-photon lithography.

1 Introduction

Metalenses, lenses composed of quasi-periodic subwavelength structures, have received a great deal of attention due to their compact size, light weight, efficient wavefront shaping, and polarization conversion properties [1–6]. On the other hand, correction of chromatic and off-axis aberrations remains challenging [7–13]. Most achromatic metalenses have been limited to either visible or near-infrared (NIR) operation [14–23]. Recent attempts to extend the corrected wavelength range have yielded broadband metalenses with diffraction-limited performance from 640 to 1200 nm [24]. However, such designs lack achromatic behavior over a significant portion of the visible spectrum and do not extend to the short-wave infrared (SWIR) limits of emerging broadband image sensors. Additionally, the aperture size of the aforementioned metasurface design is around 20 μm. The metalens dimensions may be expanded by extending the geometrical design space at the expense of fabrication difficulties and long computational time. These limitations restrict their usage in day-night vision systems, hyperspectral imaging, and other ultra-broadband applications.

In this paper, we present an achromatic metalens operating with diffraction-limited performance over almost two octaves from 450 to 1700 nm. This spectral range is well matched to visible-to-shortwave infrared image sensors that are becoming available. Achromatization is provided by phase plate and nanohole structures that are merged to a single layer lens as shown in Figure 1(a–c). Most metalenses use planar geometries and high refractive index materials. In contrast, our architecture yields high performance with low-refractive index materials by exploiting three-dimensional geometries. Our design does not require intensive computational search, and the size is not limited by the extent of the phase shift library. Unlike other techniques, achromatization is achieved with a phase shift library extending from 0 to 2π. Such a library can be easily obtained by sweeping a few geometrical parameters, which greatly reduces fabrication complexity. In our previous works, we used a variable height nanopillar metasurfaces created with two-photon lithography [25, 26]. However, these nanopillar arrays lose structural integrity when the feature size is reduced for operation at visible wavelengths. In this paper, we propose a novel nanohole structure with varying depth. Our method enables smaller feature sizes from two-photon lithography and, as a result, much broader achromatic correction.

For two-photon lithography, we use a commercial system (Nanoscribe Photonic Professional GT) operating at a wavelength of 780 nm. The metalenses were patterned in Nanoscribe's IP-DIP photoresist (n = 1.566 at 450 nm). It is

*Corresponding author: Jeffrey Todd Hastings, Electrical and Computer Engineering, University of Kentucky, Lexington, KY 40506, USA, E-mail: todd.hastings@uky.edu
Fatih Balli, Physics and Astronomy, University of Kentucky, Lexington, KY 40506, USA, E-mail: fatih.balli@uky.edu. https://orcid.org/0000-0003-4474-1284
Mansoor A. Sultan, Electrical and Computer Engineering, University of Kentucky, Lexington, KY 40506, USA, E-mail: m.sultan@uky.edu
Aytekin Ozdemir, College of Optical Sciences, University of Arizona, Tucson, AZ 85721, USA, E-mail: aytekin@email.arizona.edu

not obvious that such a system has sufficient resolution to produce metalenses operating at visible wavelengths. However, we show that judicious choice of the phase-plate and nanohole geometry leads to an experimentally accessible structure. A 0.27 numerical aperture (NA) metalens designed and fabricated with this approach exhibits a focal length shift of <6% across the entire spectral region of interest. The metalens designs also lack re-entrant features; thus, they could be molded for high volume production.

2 Theory and structure

Diffractive achromatic doublet design by recursive ray-tracing has been proposed and experimentally verified by Farn et al. [27, 28]. We recently adapted this design approach to achromatic metalenses in the near infrared region (1000–1800 nn) [25]. In this paper, we extend this approach to create a visible to short-wave infrared achromatic metalens and identify a geometry that is amenable to 3D printing via two-photon lithography.

Recursive ray-tracing uses two thin optical elements (TE) to produce a doublet corrected at two wavelengths ($\lambda_{\min}$ and $\lambda_{\max}$). Both elements must meet target phase shift requirements so that achromatization is achieved. As an approximation, the phase derivative and target phase shift values as the function of radial coordinate, r, and entrance pupil diameter (EPD) are given as

$$\phi_{\pm}^{'}(r) = \pm\phi_{o}^{'}\sqrt{1-\frac{4r^2}{\mathrm{EPD}^2}}, \tag{1}$$

and

$$\phi(r) = \frac{\pi\phi_{o}^{'}}{2}\left(2r\sqrt{1-\frac{4r^2}{\mathrm{EPD}^2}} + \mathrm{EPD}\cdot\arcsin\left(\frac{2r}{\mathrm{EPD}}\right)\right), \tag{2}$$

respectively. Figure 1(e–f) shows the phase derivative and target phase shift values for the NA = 0.27 and EPD = 20 μm metalens. We choose the operating wavelength range as $\lambda_{\min}$ = 450 nm and λ_{max} = 1700 nm. We introduce an effective thickness between TEs although two TEs are merged together and there is no physical separation between them. The maximum NA value for a given EPD is limited by the effective thickness between the TEs [25]. We choose the minimum focal length value so that ray-tracing algorithm converges. The maximum error between the ray-tracing solution and approximate formula above is 0.04 rad/μm.

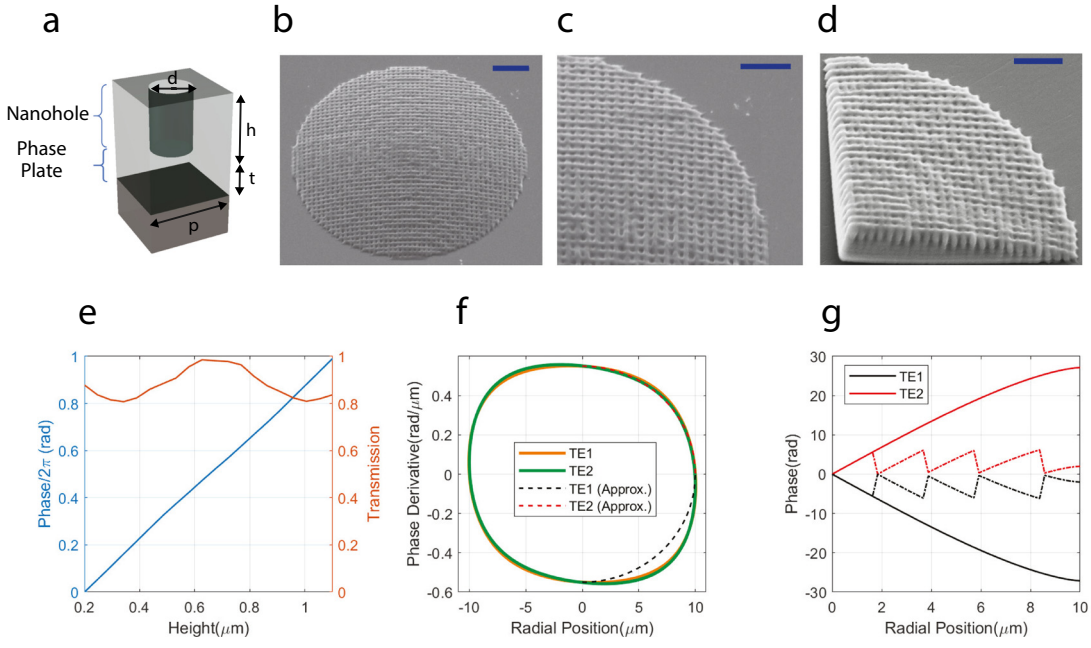

Figure 1: A 3D achromatic metalenses.
(a) The unit structure of the metalens merges a nanohole and a phase plate. The dimensions d, h, p and t represent diameter, height, and period of the nanoholes and thickness of the phase plate, respectively. We set d = 0.2 μm and p = 0.4 μm. (b) Scanning electron micrograph of 20 μm diameter metalens. The structure is fabricated with two-photon lithography on a fused silica substrate. Scale bar is 3 μm. (c) Zoomed-in image of 20 μm diameter metalens. The holes are clearly visible on the surface. (d) Quarter-section of 20 μm diameter metalens showing the varying hole depth. Scale bar is 2 μm. (e) Phase shift and transmission of nanoholes as the function of depth at 450 nm wavelength. (f, g) Phase derivative and the phase shift distribution as the function of radial coordinates for EPD = 20 μm and NA = 0.27 achromatic metalens.

The two TEs, the phase plate (bottom) and nanoholes (top), are merged into a single structure which forms the unit cell of the hybrid metalens as shown in Figure 1(a). The nanohole structure is chosen due to its higher transmission than the nanopillar [29] and advantages for fabrication. Specifically, the nanohole architecture prevents pattern distortion and collapse that can accompany high aspect ratio pillars. Figure 1(d) shows the phase shift library as the function of depth of the nanoholes under the assumption of locally periodic structure [30]. We limit the depth of the nanoholes to 0.8 μm because of fabrication constraints. The remaining phase shift is achieved by the phase plate structure.

The phase shift through a phase plate is expressed by the well-known formula $\phi(r) = \frac{2\pi(n-1)t}{\lambda_{\min}}$ where t, n are thickness and refractive index at $\lambda = \lambda_{\min}$, respectively. The period, p, is chosen to be 0.4 μm so that only zeroth-order diffraction is present and the Nyquist criteria $\left(p < \frac{\lambda}{2NA}\right)$ is satisfied. In addition to the nanohole and phase plate structures, we also add extra thickness in the hyperbolic form of $t = \frac{1}{n-1}\left(\sqrt{f^2 + \frac{\mathrm{EPD}^2}{4}} - \sqrt{f^2 + r^2}\right)$. For the 20-μm diameter metalens, the powers of the hyperbolic layer and metastructure are 0.0222 and 0.0048 μm^{-1}, respectively. Despite increasing the total thickness, this extra layer has two distinct advantages. First, we can obtain higher NA values for which recursive ray-tracing would not normally converge. Second, chromatic aberration through the hyperbolic layer is proportional to the wavelength. This differs from the residual chromatic aberration of the ray-tracing solution where the chromatic aberration is inversely proportional to the wavelength. Addition of the extra layer allows us to fully cancel chromatic aberration at two different wavelength so that achromatization is achieved.

3 Experimental results

To test our designs, we fabricated two different lenses having EPD = 20, 200 μm and NA = 0.27, 0.04, respectively. The lenses were fabricated on 0.7 mm thick fused-silica substrates using "dip-in" multi-photon lithography. Multi-photon lithography exploits two-photon cross-linking in the focal volume of an ultrafast laser pulse to create true 3D structures in a single process step [31, 32]. Fabricated metalenses are shown Figure 1b, c. Lenses were characterized using a collimated beam from a supercontinuum source.

Figure 2a illustrates measured power intensity distributions in y–z plane and intensity distribution at the focal plane. Figure 2b compares normalized power intensity profiles at the focal plane and the diffraction-limited Airy disk pattern. We define the focal plane as the z-coordinate of the maximum measured power intensity on top of the metalens. The measured focusing efficiency as a function of wavelength is shown in Figure 2c. Focusing efficiency is defined as the ratio of integrated power within the circle having radius 1.5 × FWHM to the incident power on the metalens. The average efficiency values are 60 and 42% for 20 and 100 μm lenses, respectively. Comparison of measured and diffraction-limited full-width at half-maximum (FWHM) at the focal plane is also provided in Figure 2d. Diffraction limited performance is clear from the plot. The focusing error versus wavelength is shown in Figure 2e. We define the focusing error as the normalized difference between the nominal and the measured focal length. The maximum deviation from the mean focal length is measured as 6% showing that the metalens has effectively corrected chromatic aberration over the entire visible to short-wave IR bandwidth.

We tested the imaging performance of EPD = 200 μm and NA = 0.04 metalens using the standard 1951 United States Air Force (USAF) target. Details of the experiment are explained in the supplementary information. Figure 3a shows the imaging results for group 5 (where 5–4 represents 45.3 line pairs/mm). Achromatic performance can be seen from the images taken under broadband (450–1700 nm) and SWIR (1000–1700 nm) illumination. We use a long-pass filter for the second image where wavelengths shorter than 1000 nm are filtered out. Practical usage of the metalens over the entire bandwidth is revealed by the Lego image in Figure 3(b). The SWIR and visible wavelength regimes were also separately tested as shown in Figure 3c–f.

4 Discussion and conclusion

Despite this excellent overall performance, we observe a reduction in focusing efficiency as the wavelength moves from the SWIR to the visible regime. The metalens' period plays a major role in maximizing the efficiency and transmission; as a result, higher efficiency may be obtained from similar designs employing finer periods. Shorter wavelengths are also more sensitive to fabrication imperfections, which may account for some additional reduction in performance. Further advances in two-photon lithography or a transition to gray-scale e-beam lithography may alleviate this while preserving the metalens' 3D geometry.

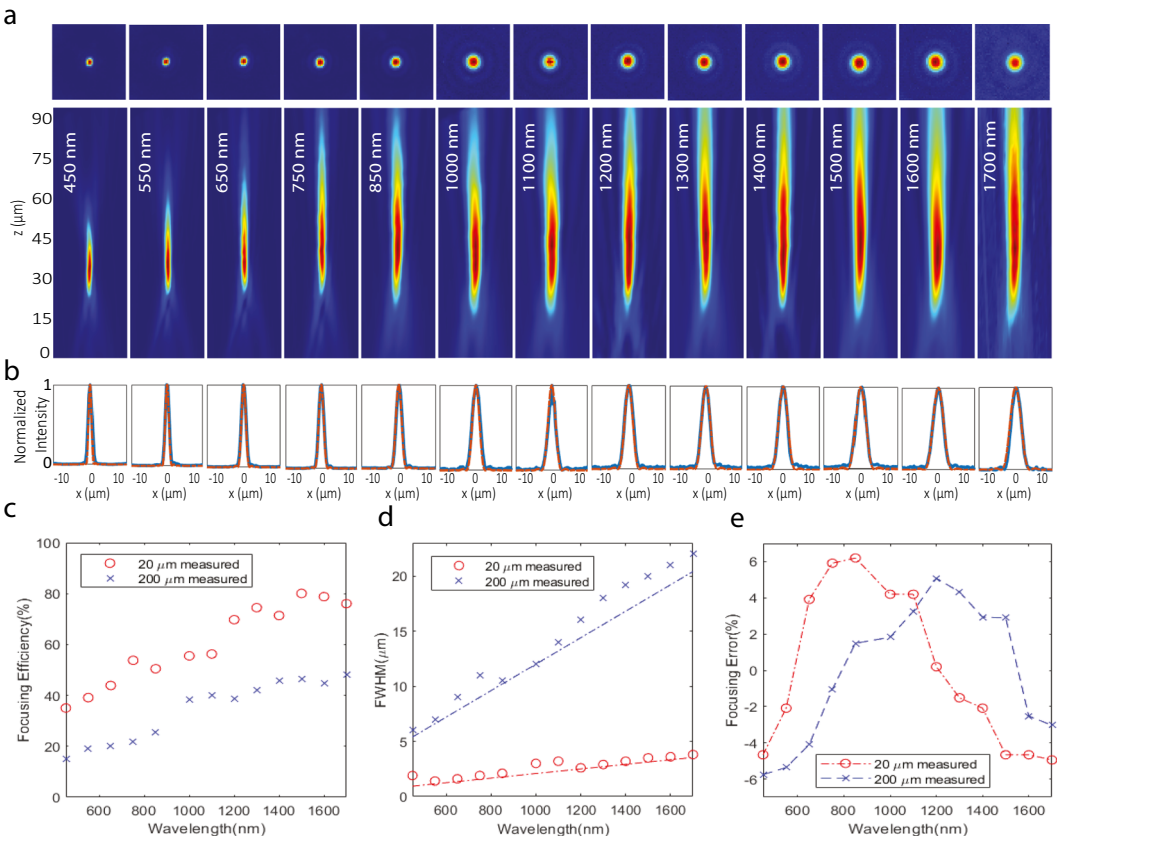

Figure 2: Experimentally measured performance of the metalens.
(a) Power intensity distribution in the x–y focal plane (upper) and x–z (lower) planes. Maximum power intensity appears around the focal plane at $z \approx 36$ μm. (b) Comparison of diffraction-limited Airy function (dashed red lines) and the measured power intensity across the focal plane (solid blue curve). We normalize the Airy fit so that the maximum intensity is unity. (c) Measured focusing efficiency as a function of wavelength. (d) Comparison of measured full-width at half-maximum (FWHM) with the diffraction limit. Dashed lines represent diffraction-limited performance. (e) Focal length error versus wavelength. Corresponding focal plane distances are 36 and 2600 μm for the 20 and 200 μm aperture size lenses, respectively.

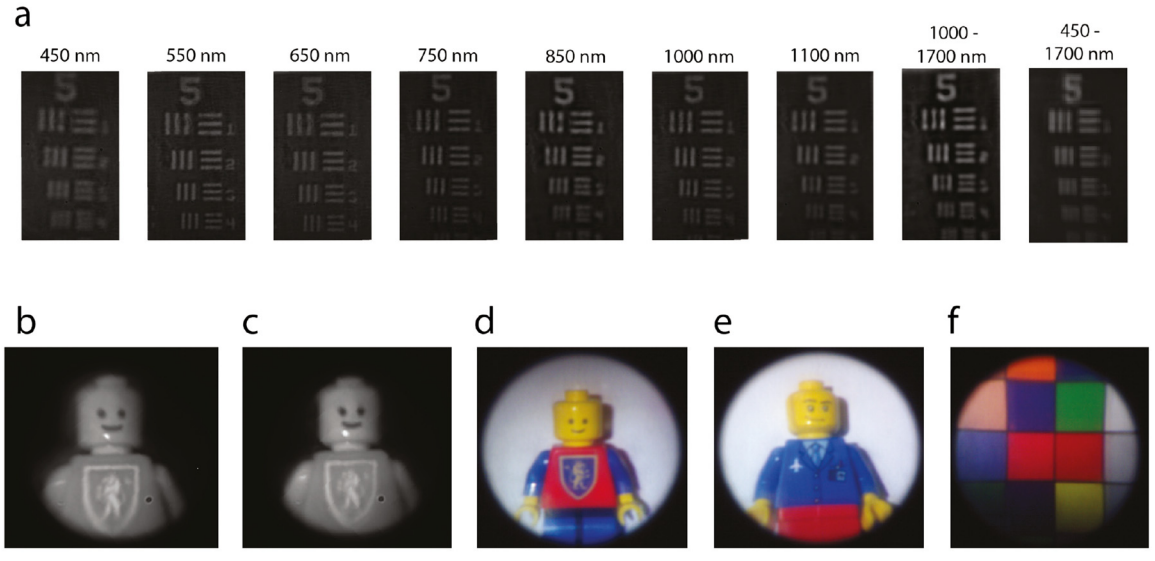

Figure 3: Imaging with EPD = 200 μm, NA = 0.04 metalens under halogen lamp illumination.
(a) Standard USAF target images for several wavelengths. (b, c) Images taken under illumination with wavelength ranges 450–1700 nm and 1000–1700, respectively. (d–f) Images taken by a color camera sensitive to visible spectrum.

Regardless, nanohole structures proved to have distinct advantages compared to nanopillars. First, nanoholes offer higher transmission as expected [29]. Equally important, nanoholes reduced fabrication difficulties making sub-wavelength structures with higher aspect ratios accessible for operation with visible light. Finally, the nanohole-phase plate geometry should be replicable by molding for mass production. Thus, 3D metalenses based on nanoholes are excellent candidates when achromatic diffraction-limited focusing and imaging is required over the entire visible to short-wave IR spectrum.

Author contributions: All the authors have accepted responsibility for the entire content of this submitted manuscript and approved submission.

Research funding: This work was partially supported by Intel Corp. The authors thank the UK Center for Nanoscale Science and Engineering, a member of the National Nanotechnology Coordinated Infrastructure (NNCI), which is supported by the National Science Foundation (ECCS-2025075). This work used equipment supported by National Science Foundation Grant No. CMMI-1125998.

Conflict of interest statement: The authors declare no conflicts of interest regarding this article.

References

[1] S. Jahani and Z. Jacob, "All-dielectric metamaterials," *Nat. Nanotechnol.*, vol. 11, p. 23, 2016.

[2] N. Yu and F. Capasso, "Flat optics with designer metasurfaces," *Nat. Mater.*, vol. 13, p. 139, 2014.

[3] P. Lalanne and P. Chavel, "Metalenses at visible wavelengths: Past, present, perspectives," *Laser Photonics Rev.*, vol. 11, p. 1600295, 2017.

[4] N. Yu, P. Genevet, M. A. Kats, et al., "Light propagation with phase discontinuities: Generalized laws of reflection and refraction," *Science*, vol. 334, p. 333, 2011.

[5] H.-T. Chen, A. J. Taylor, and N. Yu, "A review of metasurfaces: Physics and applications," *Rep. Prog. Phys.*, vol. 79, p. 076401, 2016.

[6] F. Balli, M. A. Sultan, and J. T. Hastings, "Rotationally tunable polarization-insensitive metasurfaces for generating vortex beams," in *Metamaterials, Metadevices, and Metasystems 2020*, SPIE, p. 11460, 2020.

[7] M. Khorasaninejad, W. T. Chen, R. C. Devlin, J. Oh, A. Y. Zhu, and F. Capasso, "Metalenses at visible wavelengths: Diffraction-limited focusing and subwavelength resolution imaging," *Science*, vol. 352, p. 1190, 2016.

[8] N. Meinzer, W. L. Barnes, and I. R. Hooper, "Plasmonic meta-atoms and metasurfaces," *Nat. Photonics*, vol. 8, p. 889, 2014.

[9] E. Arbabi, A. Arbabi, S. M. Kamali, Y. Horie, and A. Faraon, "Multiwavelength metasurfaces through spatial multiplexing," *Sci. Rep.*, vol. 6, p. 32803, 2016.

[10] M. Khorasaninejad, A. Y. Zhu, C. Roques-Carmes, et al., "Polarization-insensitive metalenses at visible wavelengths," *Nano Lett.*, vol. 16, p. 7229, 2016.

[11] A. Arbabi, Y. Horie, M. Bagheri, and A. Faraon, "Dielectric metasurfaces for complete control of phase and polarization with subwavelength spatial resolution and high transmission," *Nat. Nanotechnol.*, vol. 10, p. 937, 2015.

[12] A. Arbabi, E. Arbabi, S. M. Kamali, Y. Horie, S. Han, and A. Faraon, "Miniature optical planar camera based on a wide-angle metasurface doublet corrected for monochromatic aberrations," *Nat. Commun.*, vol. 7, p. 13682, 2016.

[13] A. Özdemir, Z. Hayran, Y. Takashima, and H. Kurt, "Polarization independent high transmission large numerical aperture laser beam focusing and deflection by dielectric Huygens' metasurfaces," *Optic Commun.*, vol. 401, p. 46, 2017.

[14] B. Groever, W. T. Chen, and F. Capasso, "Meta-lens doublet in the visible region," *Nano Lett.*, vol. 17, p. 4902, 2017.

[15] M. Khorasaninejad, Z. Shi, A. Y. Zhu, et al., "Achromatic metalens over 60 nm bandwidth in the visible and metalens with reverse chromatic dispersion," *Nano Lett.*, vol. 17, p. 1819, 2017.

[16] S. Shrestha, A. C. Overvig, M. Lu, A. Stein, and N. Yu, "Broadband achromatic dielectric metalenses," *Light Sci. Appl.*, vol. 7, p. 85, 2018.

[17] W. T. Chen, A. Y. Zhu, V. Sanjeev, et al., "A broadband achromatic metalens for focusing and imaging in the visible," *Nat. Nanotechnol.*, vol. 13, p. 220, 2018.

[18] W. T. Chen, A. Y. Zhu, J. Sisler, Z. Bharwani, and F. Capasso, "A broadband achromatic polarization-insensitive metalens consisting of anisotropic nanostructures," *Nat. Commun.*, vol. 10, p. 355, 2019.

[19] S. Wang, P. C. Wu, V.-C. Su, et al., "Broadband achromatic optical metasurface devices," *Nat. Commun.*, vol. 8, p. 187, 2017.

[20] S. Wang, P. C. Wu, V.-C. Su, et al., "A broadband achromatic metalens in the visible," *Nat. Nanotechnol.*, vol. 13, p. 227, 2018.

[21] S. Colburn, A. Zhan, and A. Majumdar, "Metasurface optics for full-color computational imaging," *Sci. Adv.*, vol. 4, p. eaar2114, 2018.

[22] M. Khorasaninejad, F. Aieta, P. Kanhaiya, et al., "Achromatic metasurface lens at telecommunication wavelengths," *Nano Lett.*, vol. 15, p. 5358, 2015.

[23] F. Presutti and F. Monticone, "Focusing on bandwidth: Achromatic metalens limits," *Optica*, vol. 7, p. 624, 2020.

[24] A. Ndao, L. Hsu, J. Ha, J.-H. Park, C. Chang-Hasnain, and B. Kanté, "Octave bandwidth photonic fishnet-achromatic-metalens," *Nat. Commun.*, vol. 11, pp. 1–6, 2020.

[25] F. Balli, M. Sultan, S. K. Lami, and J. T. Hastings, "A hybrid achromatic metalens," *Nat. Commun.*, vol. 11, p. 1, 2020.

[26] M. A. Sultan, F. Balli, D. L. Lau, and J. Hastings, "Hybrid metasurfaces for simultaneous focusing and filtering," *Optic Lett.*, vol. 46, p. 214, 2020.

[27] M. W. Farn and J. W. Goodman, "Diffractive doublet corrected on-axis at two wavelengths," in *1990 Intl Lens Design Conf*, G. N. Lawrence, Ed., Monterey, United States, 1991, p. 24.

[28] M. W. Farn and J. W. Goodman, "Diffractive doublets corrected at two wavelengths," *J. Opt. Soc.*, vol. 8, p. 860, 1991.

[29] N. Yilmaz, A. Ozer, A. Ozdemir, and H. Kurt, "Nanohole-based phase gradient metasurfaces for light manipulation," *J. Phys. Appl. Phys.*, vol. 52, p. 205102, 2019.

[30] R. Pestourie, C. Pérez-Arancibia, Z. Lin, W. Shin, F. Capasso, and S. G. Johnson, "Inverse design of large-area metasurfaces," *Optic Express*, vol. 26, p. 33732, 2018.
[31] S. Maruo, O. Nakamura, and S. Kawata, "Three-dimensional microfabrication with two-photon-absorbed photopolymerization," *Optic Lett.*, vol. 22, p. 132, 1997.
[32] G. von Freymann, A. Ledermann, M. Thiel, et al., "Three-dimensional nanostructures for photonics," *Adv. Funct. Mater.*, vol. 20, p. 1038, 2010.

Supplementary Material: The online version of this article offers supplementary material (https://doi.org/10.1515/nanoph-2020-0550).